Enhancing the Efficiency of Organic Solar Cell By Incorporating Copper Nanoparticles in PEDOT:PSS

Thapelo Ephraim Seimela¹

https://orcid.org/0000-0001-9961-4106

Nolwazi Nombona²

https://orcid.org/0000-0002-9946-2568

Justine Sageka Nyarige¹

https://orcid.org/0000-0002-5030-9247

Mmantsae Diale¹

https://orcid.org/0000-0002-6035-6688 mmantsae.diale@up.ac.za

Abstract

The performance of bulk heterojunction organic solar cell can be enhanced by incorporating plasmonic copper nanoparticles. In this study, a device with the architecture ITO/PEDOT:PSS:CuNPs/P3HT:PCBM/Ag was fabricated, where PEDOT:PSS was treated with copper nanoparticles synthesised by chemical reduction. Transmission electron microscopy revealed spherical copper nanoparticles with increasing average particle size as the concentration of copper sulphate increases. A face-centred cubic structure with (111), (200) and (220) phases for copper nanoparticles was confirmed using X-ray diffraction. The incorporation of copper nanoparticles induced the plasmonic resonance at 562 nm resulting in light scattering, which was not observed for pristine PEDOT:PSS. The copper nanoparticles are uniformly dispersed in PEDOT:PSS as displayed by scanning electron microscopy. The increase in concentration and annealing temperature of copper nanoparticles improved the intensity of $C_{\alpha} = C_{\beta}$ vibration mode for PEDOT:PSS and P3HT:PCBM. Incorporating copper nanoparticles in PEDOT:PSS has improved the power conversion efficiency of ITO/PEDOT:PSS:CuNPs/P3HT:PCBM/Ag solar cell from 0.09 to 5.44% as a result of the induced plasmonic resonance observed in the ultraviolet-visible spectra.

Keywords: CuNPs; solar cell; light scattering; PEDOT:PSS; P3HT:PCBM.

² Department of Chemistry, University of Pretoria, South Africa.







¹ Department of Physics, University of Pretoria, South Africa.

1 Introduction

Metal-polymer nanocomposites, which consist of metal nanoparticles (NPs) incorporated into a conducting polymer, have generated much interest for the last two decades or so because of their tuneable electrical [1], mechanical [2], magnetic [3] and optical [4] capabilities. These nanocomposites have been used in different applications, such as capacitors [5], solar cells [6], light-emitting diodes [7] and sensors [8], because of their attractive properties, including enhanced thermal stability [9], membrane permeability [10], good mechanical behaviour [11], high photocatalytic activity [12] and high optical absorption [13], [14]. Poly(3,4-ethylene dioxythiophene):poly(styrene sulphonate) (PEDOT:PSS) is a conducting polymer with a work function of 5 eV [15] and frequently used as a buffer layer in organic solar cells (OSCs) between the anode [16] and the photoactive layer (PAL) [17]. Su *et al.* [18] used PEDOT:PSS as an anode buffer layer in copper phthalocyanine (CuPc)/fullerene-based solar cell with the structure ITO/PEDOT:PSS/CuPc/C60/4,7-diphenyl-1,10-phenanthroline/Al, which gave a power conversion efficiency (PCE) between 1.15% and 1.43%.

OSCs are a rapidly developing photovoltaic (PV) technology, which offer advantages such as lightweight, mechanical flexibility, low-cost [19] and solution-processed fabrication [20]. Nanostructures can enhance the conductivity of PAL in OSCs by band engineering, light absorption and carrier separation, and prevent fast exciton recombination. Shen et al. incorporated copper nanoparticles (CuNPs) in OSCs with the structure ITO/PEI/P3HT:ICBA/WO₃:CuNPs/Ag, which showed an increase in PCE from 4.65% to 5.36% [21]. In another experiment, Liu et al. [22] incorporated CuNPs inside the PEDOT:PSS layer of OSC and they observed improvement in PCE from 3.58% to 3.96% for ITO/PEDOT:PSS:CuNPs/P3HT:PC60BM/Al device and from 6.79% to 7.43% for ITO/PEDOT:PSS:CuNPs/PTB7:PC70BM/Al device. Huang et al. multilayered incorporating [23] fabricated OSCs. by **CuNPs** ITO/PEDOT:PSS/P3HT:PC61BM:CuNPs/Ca/A1 and ITO/PEDOT:PSS/PBDTTT-EFT:PC₇₁BM:CuNPs/Ca/Al, which showed improvements in PCE of 3.26–3.43% and 6.35–7.28% respectively. Ng et al. [24] incorporated gold (Au) nanospheres (NSs), nanorods (NRs) and nanocubes (NCs) individually in different OSCs, and increased the PCE from 7.5% for pristine device to 8.0%, 8.1% and 8.2% respectively. The gold nanoclusters (AuNCs) in their device showed increased PCE due to improved light absorption in a broad wavelength region of 400-700 nm. Table I summarises the OSCs fabricated by previous researchers along with their performance.

Adding sub-wavelength-dimension metal NPs to PEDOT:PSS sheets have been found to increase the composite's absorption in the visible spectrum because of localised surface plasmon resonance (LSPR) [25]–[27], as opposed to embedding the NPs in the PAL [28], [29]. In the past, much focus about plasmonic solar cells was on noble metal NPs such as Au and silver (Ag) because of their high stability. However, the cost of these noble metals is high. This can influence the cost of OSCs and negatively affect their commercialisation. Cu is more abundant and costs less than Au and Ag. The

application of CuNPs might be the desirable solution since they also have LSPR in the visible spectrum [23], [30].

TABLE I SUMMARY OF OSCS AND THEIR PCE

Structure	NPs	PCE (%)	Ref.
ITO/ZnO:CuNPs/P3HT:PCBM/MoO ₃ /Ag	Cu	2.74	[18]
ITO/PEI/P3HT:ICBA/WO3:CuNPs/Ag	Cu	5.36	[21]
ITO/PEDOT:PSS:CuNPs/P3HT:PC60BM/A1	Cu	3.96	[22]
ITO/PEDOT:PSS:CuNPs/PTB7:PC70BM/Al	Cu	7.43	[22]
ITO/PEDOT:PSS/P3HT:PC ₆₁ BM:CuNPs/Ca/Al	Cu	3.43	[23]
ITO/PEDOT:PSS/PBDTTT-EFT:PC71BM:CuNPs/Ca/Al	Cu	7.28	[23]

In addition, it has been noted that adding CuNPs to PEDOT:PSS can increase both the material's conductivity and surface roughness [20]. Surface roughness improves incident light scattering while decreasing reflection-related losses. Owing to their superior optical, structural and electrical characteristics, hybrid CuNPs-PEDOT:PSS thin films have the potential to enhance the photovoltaic performance of OSCs [31].

In this study, colloidal CuNPs were synthesised by chemical reduction and incorporated in PEDOT:PSS within the OSC. The effects of varying their concentration showed a LSPR with a wider wavelength and tunability in the visible spectrum, which indicates improved light absorption.

2 Experimental Method

2.1 Materials

Ascorbic acid (AA), polyvinyl pyrrolidone (PVP), trisodium citrate ($Na_3C_6H_5O_7$), sodium hydroxide (NaOH), sodium borohydride (NaBH₄), copper(II) sulphate pentahydrate (CuSO₄.5H₂O), and P3HT:PC₆₁BM were all obtained from Sigma Aldrich and used as received. The 20 mm \times 15 mm indium tin oxide (ITO) coated glass substrates and PEDOT:PSS were obtained from Ossila.

2.2 Synthesis of Copper Nanoparticles

Citrate-capped CuNPs were synthesised using a method developed by Dang *et al.* [32]. Briefly, 52.8 mg of AA was dissolved in 15 mL of deionised (DI) water. Under vigorous stirring, 0.01 M CuSO₄ solution was added to the AA. PVP (0.01 M) was added to CuSO₄ at three different ratios. After 1 hour of stirring at room temperature, 0.1 M NaBH₄ was added to the mixture and followed by vigorous stirring for 10 minutes. NaOH (1 M) was added to the resultant solution dropwise until the pH reached 12. The colour of the reaction changed from blue to yellow, then pale brown.

The CuNPs were separated and rinsed with DI water. Excess PVP was removed using acetone. The precipitates were dried for 4 hours [32].

2.3 Substrate Cleaning

ITO pre-patterned glass substrates were cleaned by soaking in NaOH solution for 10 minutes and then rinsed in DI water [33]. After cleaning, the substrates were soaked in ethanol and then agitated for 10 minutes in an ultrasonic bath. The substrates were rinsed in DI water, soaked in acetone, rinsed again, and then dried using nitrogen gas [33]. The cleaned substrates were placed in a UV ozone cleaner for 15 minutes to increase wettability.

2.4 Fabrication of Solar Cell

PEDOT:PSS was first filtered through a hydrophilic filter before being spin-coated on ITO glass at 3 000 rpm for 30 s. The first solution was pristine PEDOT:PSS whereas the others contained varied volumes of CuNPs. The annealing temperature for the thin films was 120 °C for 15 min which were then allowed to cool to room temperature. P3HT and PCBM were dissolved in dichlorobenzene with a molar ratio of 1:1 and stirred with a magnetic stirrer for 12 hours. The P3HT:PCBM blend was spin-coated on top of PEDOT:PSS at 3 000 rpm for 30 s and annealed at 120 °C for 5 min. The samples were put in a corning glass desiccator for 24 hours, to allow natural drying. Then 100 nm thick Ag contacts were thermally evaporated at a working pressure of 4.5×10^{-6} mbar and a deposition rate of 0.1 Å/s using a resistive evaporator. The schematic diagram of the OSC fabricated is illustrated in Fig. 1.

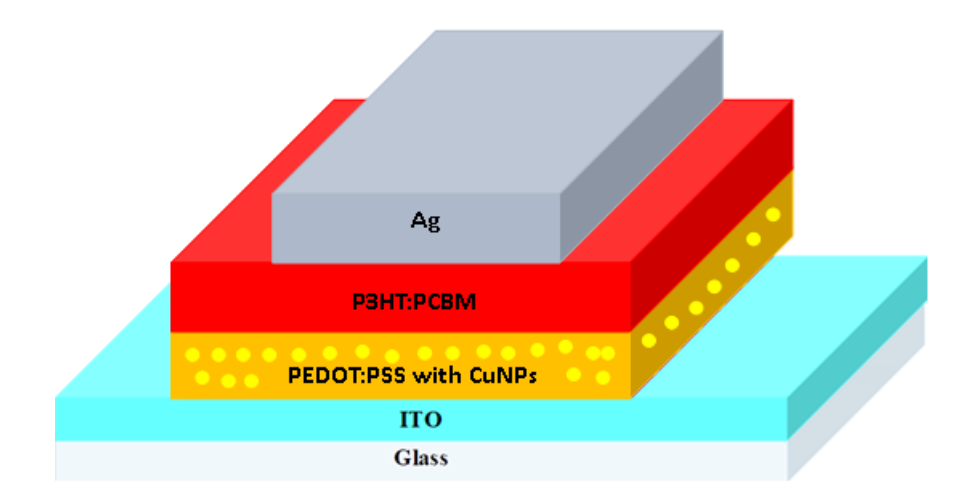


Fig. 1. Schematic diagram of OSC incorporated with CuNPs in the PEDOT:PSS.

2.5 Characterisation

The morphology of CuNPs was determined using field emission gun transmission electron microscopy (FEG-TEM, Jeol 2100). The morphology of PEDOT:PSS and P3HT:PCBM was determined using field emission scanning electron microscopy (FESEM Zeiss Ultra PLUS microscopy). The particle sizes of the NPs were measured from the TEM and SEM micrographs using ImageJ software. Agilent Cary 60 Bio UV-Vis spectrophotometer was used to measure the absorption of the particles. X-ray diffraction patterns were obtained using a German Bruker D2 PHASER X-ray diffractometer with a CuKα radiation (1.5418 Å) source. Raman spectroscopy was performed using a WITec alpha300 RAS+ confocal Raman microscope with a 532 nm excitation laser. The current density–voltage (J–V) characteristics were measured under 1 000 W/m² radiation using the Ossila Solar Cell I-V Test System.

3 Results

3.1 X-Ray Diffraction

X-ray diffraction (XRD) patterns of CuNPs for different concentrations of CuSO₄ are illustrated in Fig. 2. All three samples have (111), (200) and (220) Cu peaks indexed at 42°, 49° and 74° respectively. These diffraction peaks confirm that CuNPs produced in this study have a face-centred cubic (FCC) crystal structure. The (111) peak has the highest intensity indicating the crystallinity of CuNPs. This is in agreement with Samim *et al.* [34] where they have synthesised CuNPs with different concentrations of CuSO₄. It has been established that CuNPs are vulnerable to oxidation, easily forming copper (I) oxide and copper (II) oxide that appears as a thin layer [34], [35]. The three XRD patterns show no signs of crystallographic impurities which confirms the absence of oxidation, attributed to the addition of ascorbic acid (AA) which acted as an antioxidant in the synthesis process.

Table II presents the XRD analysis of CuNPs indicating increase in crystallite size and decrease in d-spacing. The average lattice constant of CuNPs was calculated to be 0.36 nm. Suárez-Cerda *et al.* [35] synthesised CuNPs using native cyclodextrins in which they calculated the same lattice constant. Similarly, Thirugnanasambandan and Alagar [36] prepared Cu nanopowder from CuSO₄ in which they obtained the same lattice constant.

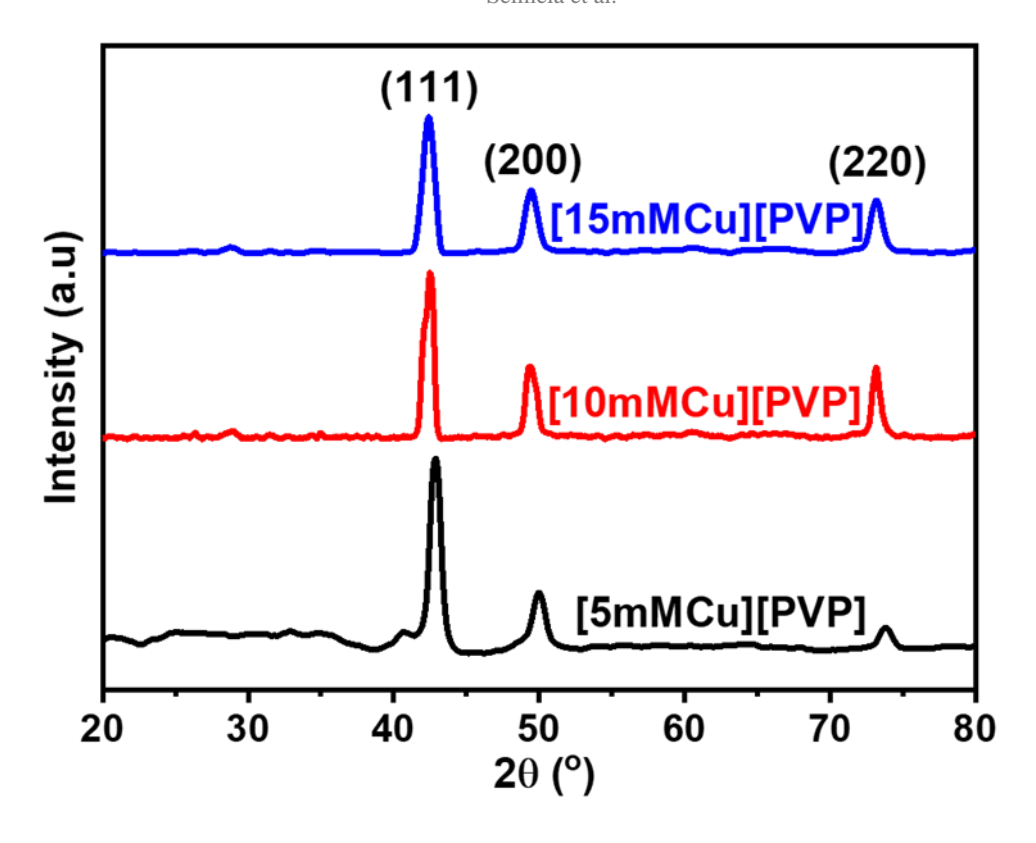


Fig. 2. XRD patterns of CuNPs at different concentrations of CuSO₄.

TABLE II XRD ANALYSIS OF THE OBTAINED Cu NPs

Sample	Peak	2θ (deg.)	β (deg.)	D (nm)	d-spacing (nm)	a (nm)
[5mMCu] [PVP]	111	42.861	0.867	9.737	0.211	0.365
	200	49.976	0.964	8.999	0.182	0.365
	220	74.480	0.714	13.823	0.127	0.360
[10mMCu] [PVP]	111	42.412	0.774	10.898	0.213	0.369
	200	49.449	0.846	10.237	0.184	0.368
	220	73.173	0.703	13.925	0.129	0.366
[15mMCu] [PVP]	111	42.395	0.914	9.226	0.213	0.369
	200	49.456	1.007	8.598	0.184	0.368
	220	73.184	0.942	10.393	0.129	0.366

3.2 Transmission Electron Microscopy

TEM images of the water-soluble CuNPs made from different concentrations of CuSO₄ are displayed in Fig. 3. CuNPs produced in this study are spherical. The average particle sizes of CuNPs containing varying concentrations of 5, 10 and 15 mM CuSO₄ are 6.01 ± 0.89 nm, 17.32 ± 0.55 nm and 32.00 ± 0.75 nm, respectively. This suggests that the difference in concentration of CuSO₄ had a major effect on the size of the CuNPs. However, this size effect is also influenced by the concentration of PVP as it is a ratio to the concentration of CuSO₄. PVP prevents aggregation of CuSO₄, acting as a polymeric capping agent as well as a size controller [32].

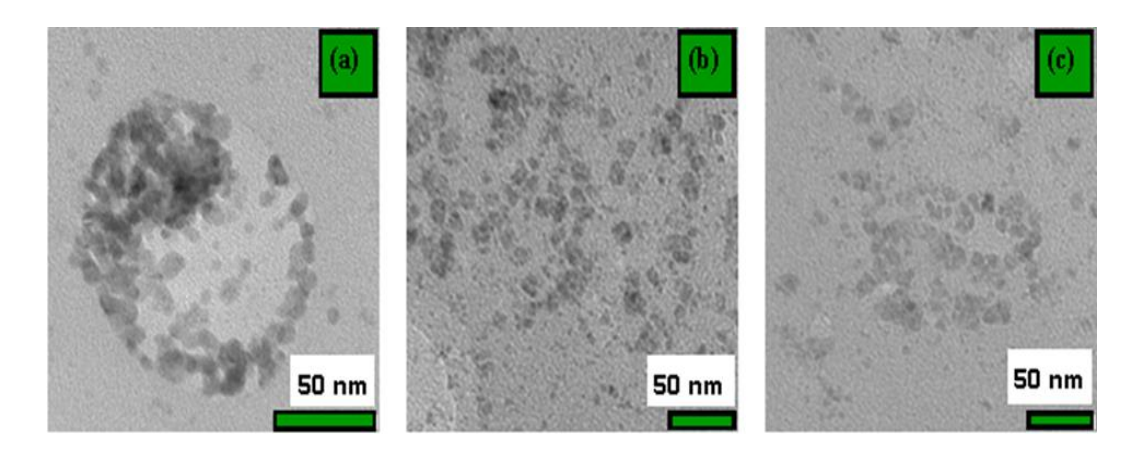


Fig. 3. TEM images of Cu NPs with AA at (a) 5 mM, (b) 10 mM and (c) 15 mM $\,$ CuSO₄.

3.3 Raman Spectroscopy

The Raman spectrum of PEDOT:PSS is illustrated in Fig. 4(a). The peaks at 997, 1 108 and 1 572 cm⁻¹ are assigned to PSS. The peaks at 449, 701, 1 267, 1 373, 1 446 and 1 511 cm⁻¹ are assigned to C–O–C and C–S–C deformations [37], C_{α} – C_{α} inter-ring stretching, C_{β} – C_{β} stretching, C_{α} = C_{β} symmetrical, and C_{α} = C_{β} asymmetrical vibrations modes for PEDOT, respectively [38]–[40].

The different volumes of CuNPs have not changed the vibrational bonds but slightly increased the intensity as shown in Fig. 4(b). The intensity increases with the increase in different volumes. However, the annealing temperatures have shown a decrease in intensity at $140~^{\circ}\text{C}$ as the pronounced peak is smaller than $120~\text{and}~160~^{\circ}\text{C}$ observed in Fig. 4(c).

The Raman spectrum of P3HT:PCBM is shown in Fig. 4(d). The intense peak at 1 467 cm⁻¹ is assigned to the $C_{\alpha} = C_{\beta}$ symmetric stretch mode while 1 390 cm⁻¹ represents C_{β} — C_{β} ; inter-ring stretch mode of the aromatic thiophene ring [41]. The peak

at 731 cm⁻¹ is assigned to C_{α} – C_{α} ring deformation [42]. The other smaller peaks (1 099, 1 217 and 1 535 cm⁻¹) are assigned to C_{β} – C_{alkyl} stretching mode, C_{β} –H stretching mode and C_{α} – C_{β} antisymmetric stretch mode, respectively [42], [43]. These results are in agreement with previous results [43].

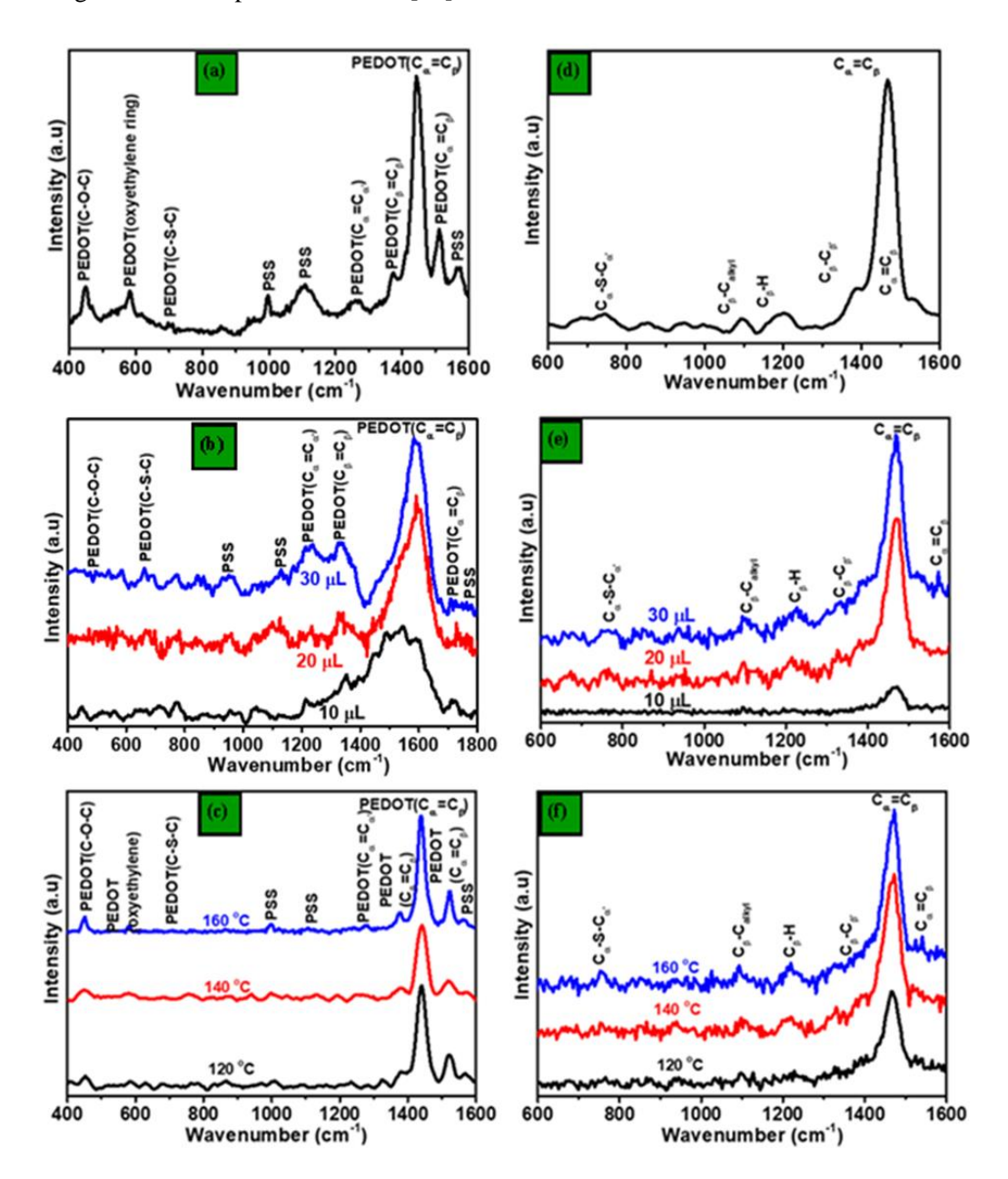


Fig. 4. Raman spectra of PEDOT:PSS for (a) pristine, (b) different volumes of CuNPs, and (c) different annealing temperatures. Raman spectra of P3HT:PCBM for (d) pristine, (e) different volumes of CuNPs, and (f) different annealing temperatures.

3.4 Ultraviolet-Visible Spectra

Ultraviolet-visible (UV-Vis) absorption spectra of CuNPs are shown in Fig. 5, with absorption bands ranging from 500–600 nm in the visible region [32], [44]. It has been reported that oxidised CuNPs absorb at 618 nm [45] and 636 nm [46]. Fig. 5(a) depicts the NPs synthesised without AA and shows the absorption peak at 740 nm. After some time this peak red shifts to 775 nm (Fig. 5(b)), which indicates oxidation. Fig. 5(c) and 5(d) shows the UV-Vis spectra of the CuNPs synthesised using AA at different CuSO₄ concentrations. The plasmonic resonance of CuNPs synthesised with AA at 5 mM CuSO₄ was 560 nm, whereas those made with 10 and 15 mM CuSO₄ were both at 562 nm. These absorption bands were not far from each other showing that the concentration did not play a role in the plasmonic resonance. Ismail [47] also observed absorption bands of CuNPs at 560 nm under the same conditions.

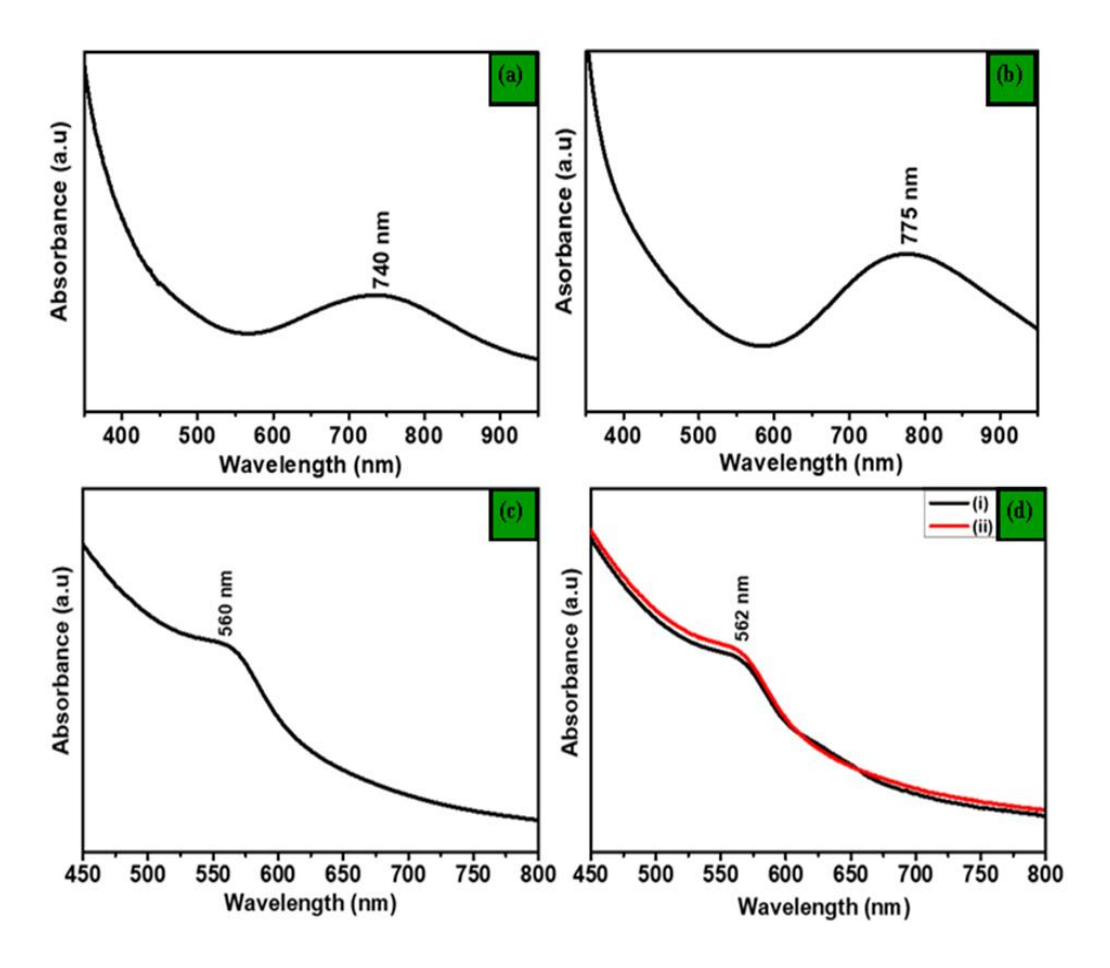


Fig. 5. UV-Vis spectra of CuNPs prepared without AA (a) immediately after synthesis, (b) after 1 day of synthesis and prepared with AA (c) 5 mM of CuSO₄, (d) (i) 10 mM of CuSO₄ and (ii) 15 mM of CuSO₄.

Fig. 6(a) and 6(b) present the UV-Vis spectra of PEDOT:PSS with and without CuNPs. The pristine PEDOT:PSS is a transparent polymer used in OSCs. This is shown by the absence of an absorption peak in Fig. 6(a). The incorporation of CuNPs decreased the PEDOT:PSS absorption since this introduced peak at 533 nm was regarded as their plasmonic resonance as shown in Fig. 6(b). The increase in the volume of CuNPs had an impact on the intensity of the absorption in the polymer. The 30 μ L volume was higher than the 10 and 20 μ L, which indicates that more CuNPs absorb more light which is good for solar cells. Otieno *et al.* [48] reported similar results when incorporating Au NPs in PPEDOT:PSS where they observed plasmonic resonance of the NPs.

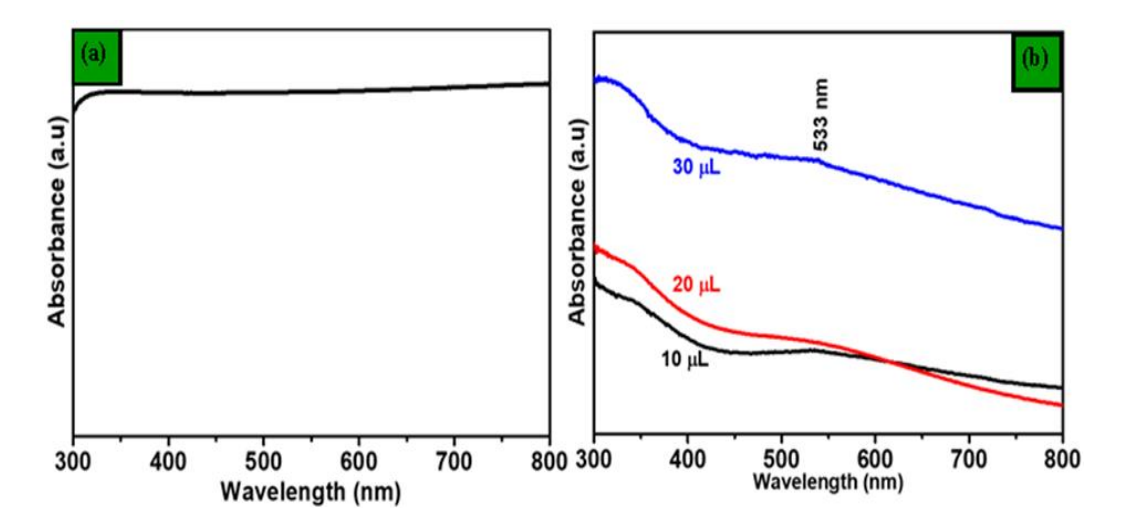


Fig. 6. UV-Vis spectra of (a) pristine PEDOT:PSS and (b) PEDOT:PSS containing different volumes of CuNPs.

The UV-Vis spectra of P3HT:PCBM are shown in Fig. 7. P3HT:PCBM resulted in a bimodal spectrum as shown in Fig. 7(a). P3HT and PCBM absorb at different wavelengths of 448 and 330 nm, respectively, which implies that P3HT absorbs in the visible range and PCBM absorbs in the UV region. According to Shaban *et al.* [49], the peak at 487 nm is attributed to band-to-band transitions deduced from π - π * transitions between the permitted highest occupied molecular orbital (HOMO) and the lowest unoccupied molecular orbital (LUMO) of P3HT:PCBM [41]. The incorporation of CuNPs in the PAL has resulted in the combination of the two peaks of P3HT and PCBM as shown in Fig. 7(b).

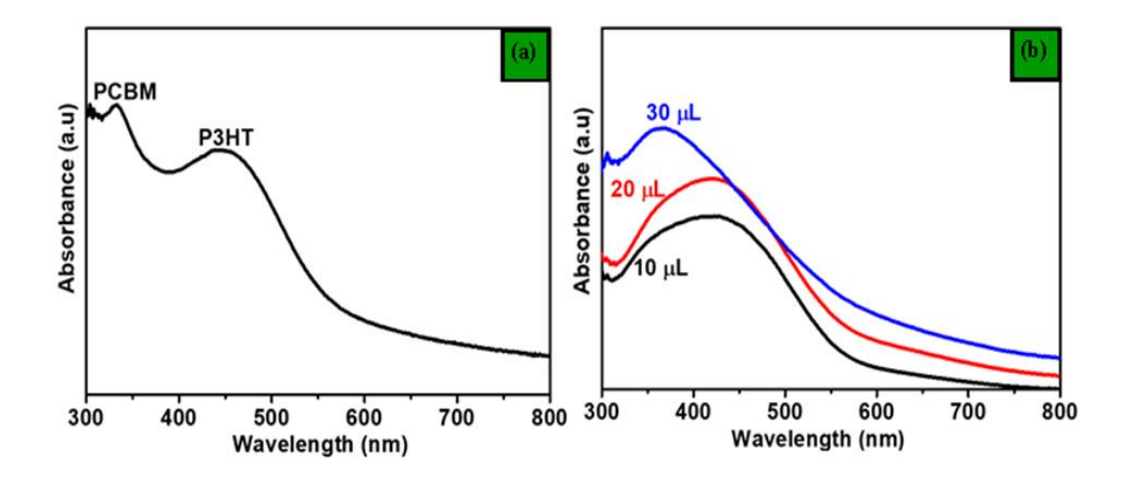


Fig. 7. UV-Vis spectra of (a) pristine P3HT:PCBM and (b) P3HT:PCBM containing different volumes of Cu NPs.

The UV-Vis absorption spectra of P3HT:PCBM annealed at different temperatures are presented in Fig. 8(a), and the absorption spectra of PEDOT:PSS with CuNPs show temperature-dependent absorption in Fig. 8(b). CuNPs are shown to produce the same broad peak between 320 and 500 nm observed in Fig. 6(b) spectra. This peak shows a minor blue shift at high annealing temperatures (> 160 °C), attributed to the heat treatment disrupting the structure and orientation for the P3HT chain ordering at 602, 550 and 510 nm, respectively. Absorption characteristics (S0, S1, S2) related to P3HT excitonic absorption were discovered. Shaban *et al.* [49] observes excitonic absorptions creating singlet exciton, exciton plus phonon, and exciton plus two phonons.

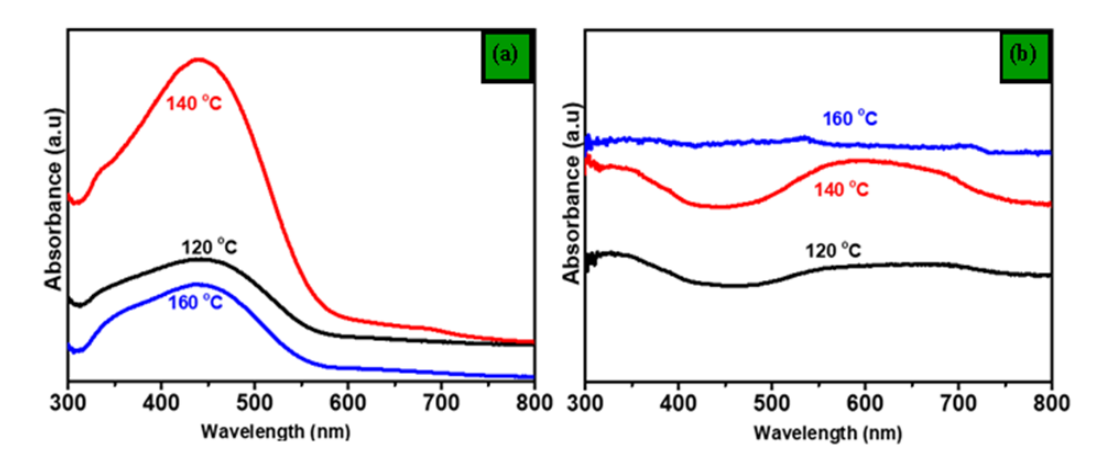


Fig. 8. UV-Vis spectra of CuNPs incorporated in (a) P3HT:PCBM and (b) PEDOT:PSS annealed at different temperatures.

3.5 Scanning Electron Microscopy

SEM images of PEDOT:PSS and P3HT:PCBM with CuNPs at different volumes are presented in Fig. 9. The images show full coverage of the polymers onto ITO without any cracks. The full coverage was influenced by the viscosity of ethanol amine, which helped PEDOT:PSS stick onto the ITO substrate. The CuNPs are not visible in any of the P3HT:PCBM polymers in Fig. 9(a) to 9(c). The different volumes of CuNPs incorporated in PEDOT:PSS can be seen in Fig. 9(d) to 9(f) as white dots. The density of the incorporated CuNPs increases with increasing CuSO₄. CuNPs are well dispersed in PEDOT:PSS, with no significant aggregation. The particles are generally spherical, with average sizes ranging from 20 to 40 nm. The NPs are uniform in size as it was the same concentration of CuSO₄ used in the preparation. The SEM results agree with Hassan *et al.* [50] who observed similar morphology when they uniformly deposited PEDOT:PSS.

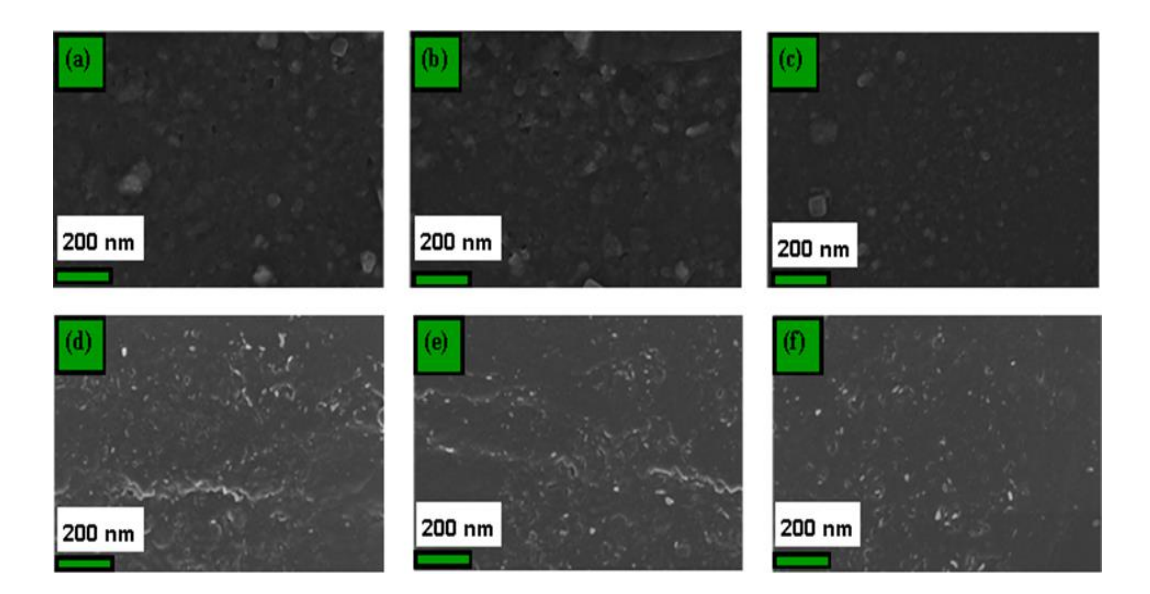


Fig. 9. SEM images of CuNPs incorporated in P3HT:PCBM for (a) 10 μ L, (b) 20 μ L and 30 μ L; and PEDOT:PSS for (d) 10 μ L, (e) 20 μ L and (f) 30 μ L.

Fig. 10(a) to 10(c) presents the SEM images of P3HT:PCBM annealed at different temperatures from 120 to 160 °C. The morphology in Fig. 10(a) to 10(c) has rough surfaces while the 160 °C became smooth. SEM images of PEDOT:PSS containing 20 μ L CuNPs annealed are presented in Fig. 10(d) to 10(f). The smooth surfaces are observed in Fig. 10(d) and 10(e). The 160 °C annealed sample has become porous as a result of the higher temperature.

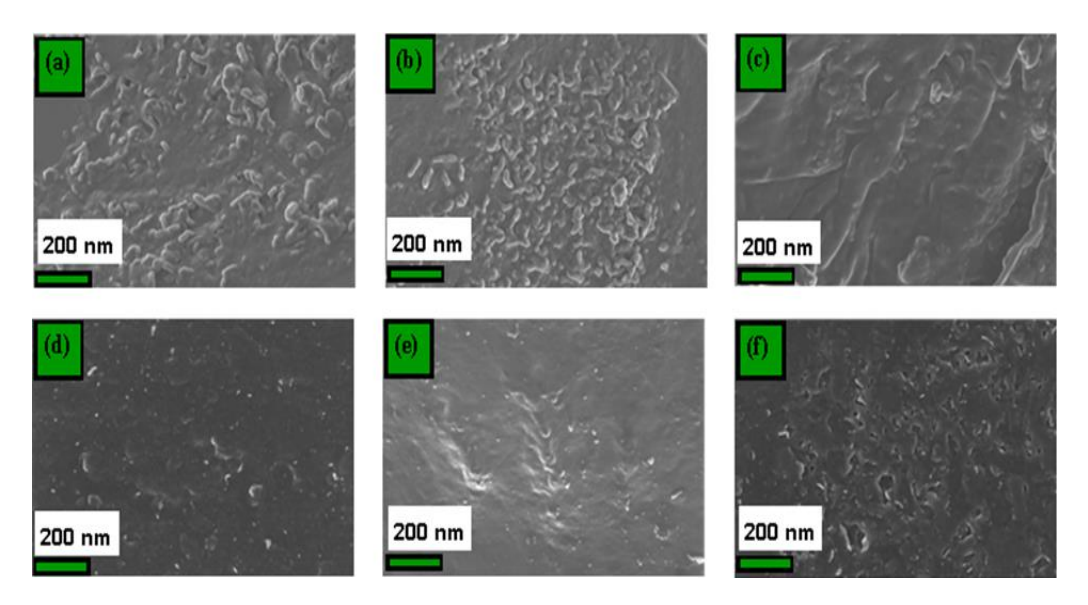


Fig. 10. SEM images of CuNPs incorporated in P3HT:PCBM at annealing temperatures of (a) 120 °C, (b) 140 °C and 160 °C; and PEDOT:PSS at annealing temperatures of (d) 120 °C, (e) 140 °C and (f) 160 °C.

3.6 Current Density-Voltage (J-V) Measurements

Fig. 11 shows the J–V characteristics of ITO/PEDOT:PSS/P3HT:PCBM/Ag OSC with varying CuNPs concentrations in PEDOT:PSS under illumination with intensity of 1 sun (1 000 Wm⁻²). The J–V graphs show an increase in J_{sc} from 1.17 to 7.86 mAcm⁻² and decrease in V_{oc} from 0.85 to 0.79 V. Incorporating CuNPs in PEDOT:PSS alters its work function, consequently improving the current density. According to Otieno *et al.* [48], the PEDOT:PSS's reduced work function is responsible for the drop in series resistance (R_s) by AuNP. This is in agreement with the 20 μ L CuNPs, which exhibit low resonant absorption intensity and strong photocurrent.

Fig. 12 shows the J–V characteristics of devices with varying CuNPs concentrations in the PEDOT:PSS layer after 1 week of fabrication. The pixel area of the device was decreased from 0.010 to 0.001 cm⁻², which resulted in the increase of J_{sc} from 10.70 to 12.86 mAcm⁻² for the 20 μ L CuNPs device. The PCE of the device with 20 μ L also increased from 5.44 to 8.77%.

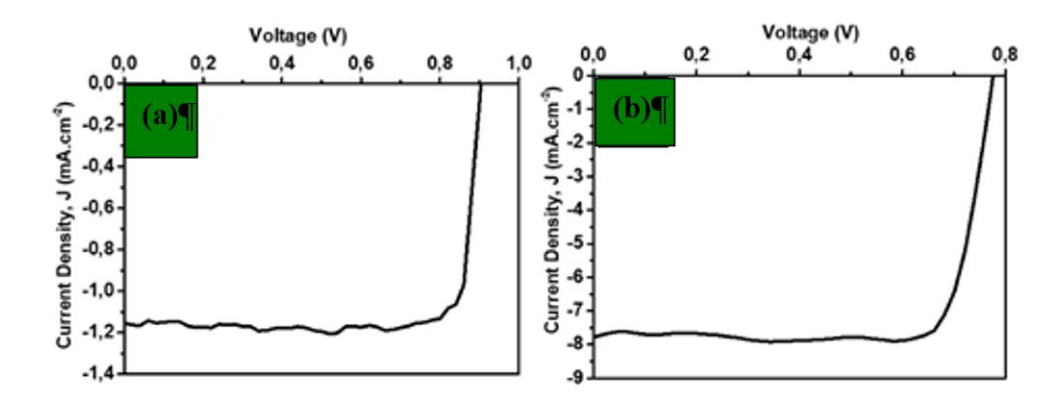


Fig. 11. J–V characteristic curves under illumination that compared the performance of OSC measured on the same day for (a) pristine and (b) 20 μL CuNPs.

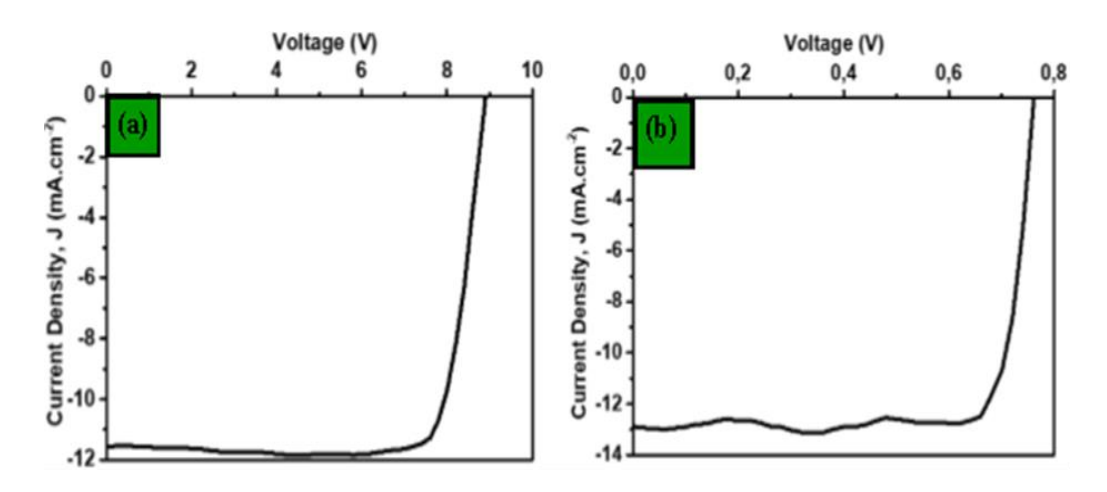


Fig. 12. J–V characteristic curves under illumination that compared the performance of OSC measured after 1 week for (a) pristine and (b) 20 μL CuNPs.

Table III lists the specific OSCs parameters in detail. The PCE from these results has shown improvement as compared to the same devices containing CuNPs a week before. The devices with higher fill factor (FF) have gained reasonable PCE.

TABLE III
AN OVERVIEW OF THE PHOTOVOLTAIC CHARACTERISTICS FOR OSCS
THAT WERE ACQUIRED USING THE J–V DATA

	Pixel	PCE (%)	FF (%)	J _{sc} (mAcm ⁻²)	Voc (V)
Fresh	Pristine	0.09	0.19	-8.58	0.85
	20 μL CuNPs	5.44	93.60	-10.70	0.84
After	Pristine	3.78	66.59	-7.86	0.72
1 week	20 μL CuNPs	8.77	87.95	-12.86	0.78

The effect of annealing temperature of the ITO/PEDOT:PSS:Cu/P3HT:PCBM/Ag OSC was investigated and is shown in Fig. 13 with the J–V characteristics. The improved OSC device displayed J_{SC} of 12.93 mAcm⁻² and V_{oc} of 0.78 V at 160 °C. The minimal change in J_{SC} at about 160 °C shows that the PAL's phase separation or breakdown is not accompanied by the rise in charge transportation. When the annealing temperature was raised from 120 to 160 °C, J_{SC} values increased from 1.10 to 12.93 mAcm⁻², which shows an increase in photon-to-current conversion efficiency. Based on the measured values of PCE, FF, V_{oc} and J_{SC} , the ideal annealing temperature for fabricating the OSC was 140 °C. Table IV outlines the OSC parameters with different annealing temperatures.

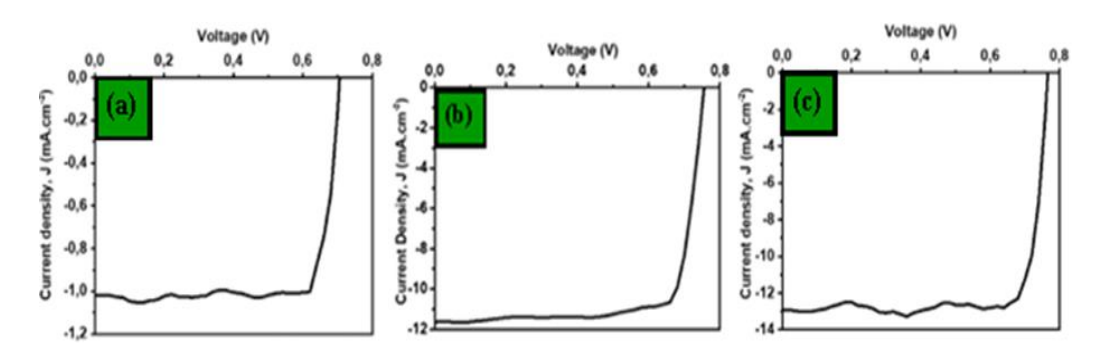


Fig. 13. J–V characteristic curves under illumination that compared the performance of OSC at annealing temperatures of (a) 120 °C, (b) 140 °C and 160 °C.

TABLE IV SUMMARY FOR PERFORMANCE OF OSC WITH VARYING ANNEALING TEMPERATURES

Pixel	PCE (%)	FF (%)	J _{sc} (mAcm ⁻²)	$V_{oc}(V)$
120°C	0.74	88.76	-1.10	0.71
140°C	0.90	27.95	-11.88	0.77
160°C	0.55	30.52	-12.93	0.78

4 Conclusion

In this study, the structural and optical properties of CuNPs in PEDOT:PSS were investigated. The CuNPs were successfully synthesised using chemical reduction in which CuSO₄ was capped separately with AA and reduced to Cu using NaBH₄ and heat. The TEM analysis confirmed the spherical shape of the NPs with an average particle size of 5.0 ± 1.2 nm for CuNPs. The FE-SEM revealed compact coverage of PEDOT:PSS showing the NPs incorporated. The UV-Vis spectra for NPs and P3HT had peaks in the visible region, whereas PCBM had a peak in the UV region. The FCC crystal structures for CuNPs were confirmed by XRD with (111), (200) and (220) peaks between 20 and 80°. The CuNPs also showed increases in PCE for the devices measured on the same day, however, the OSC having 20 μ L of CuNPs improved by 5%. After one week of fabricating the OSCs, the PCE of pristine and 20 μ L CuNPs devices have improved. Further studies can be done by synthesising different shapes and sizes of plasmonic NPs to be incorporated into PEDOT:PSS.

5 References

- [1] B. Usmani *et al.*, "Inverted PTB7-Th:PC₇₁BM organic solar cells with 11.8% PCE via incorporation of gold nanoparticles in ZnO electron transport layer," *Sol. Energy*, vol. 214, pp. 220–230, January 2021, doi: 10.1016/j.solener.2020.11.071.
- [2] X. Chen *et al.*, "Realizing ultrahigh mechanical flexibility and >15% efficiency of flexible organic solar cells via a 'welding' flexible transparent electrode," *Adv. Mater.*, vol. 32, no. 14, p. 1908478, April 2020, doi: 10.1002/adma.201908478.
- [3] D. Sharma and R. Jha, "Analysis of structural, optical and magnetic properties of Fe/Co codoped ZnO nanocrystals," *Ceram. Int.*, vol. 43, no. 11, pp. 8488–8496, August 2017, doi: 10.1016/j.ceramint.2017.03.201.
- [4] Z. Zheng et al., "A highly efficient non-fullerene organic solar cell with a fill factor over 0.80 enabled by a fine-tuned hole-transporting layer," Adv. Mater., vol. 30, no. 34, p. 1801801, August 2018, doi: 10.1002/adma.201801801.
- [5] V. Anju and S. K. Narayanankutty, "High dielectric constant polymer nanocomposite for embedded capacitor applications," *Mater. Sci. Eng.*, B, vol. 249, p. 114418, October 2019, doi: 10.1016/j.mseb.2019.114418.
- [6] Z. Liu, J. Park, B. Li, H. P. Chan, D. K. Yi and E.-C. Lee, "Performance improvement of organic bulk-heterojunction solar cells using complementary plasmonic gold nanorods," *Org. Electron.*, vol. 84, p. 105802, September 2020, doi: 10.1016/j.orgel.2020.105802.
- [7] A. de Morais, W. de Souza Rodrigues, D. J. Coutinho, A. F. Nogueira and J. N. de Freitas, "Investigation of nitrogen-doped carbon dot/ZnO nanocomposites and their application as interlayer in solution-processed organic light emitting diodes," *Mater. Sci. Eng.*, *B*, vol. 297, p. 116749, November 2023, doi: 10.1016/j.mseb.2023.116749.

- [8] A. Zinovičius, "Formation of metal-biomaterials nanocomposites and their application for the development of immunosensors," PhD dissertation, Vilnius Tech, 2024, doi: 10.20334/2024-025-M.
- [9] L. Duan and A. Uddin, "Progress in stability of organic solar cells," *Adv. Sci.*, vol. 7, no. 11, p. 1903259, June 2020, doi: 10.1002/advs.201903259.
- [10] A. Rabajczyk, M. Zielecka, K. Cygańczuk, Ł. Pastuszka and L. Jurecki, "Nanometals-containing polymeric membranes for purification processes," *Materials*, vol. 14, no. 3, p. 513, January 2021, doi: 10.3390/ma14030513.
- [11] Z. Rahimi-Ahar and L. Rahimi Ahar, "Thermal, optical, mechanical, dielectric, and electrical properties of nanocomposites," *Eur. Polym. J.*, vol. 218, p. 113337, September 2024, doi: 10.1016/j.eurpolymj.2024.113337.
- [12] T. K. Das, M. Jesionek, Y. Çelik and A. Poater, "Catalytic polymer nanocomposites for environmental remediation of wastewater," *Sci. Total Environ.*, vol. 901, p. 165772, November 2023, doi: 10.1016/j.scitotenv.2023.165772.
- [13] M. S. A. Darwish, M. H. Mostafa and L. M. Al-Harbi, "Polymeric nanocomposites for environmental and industrial applications," *Int. J. Mol. Sci.*, vol. 23, no. 3, January 2022, doi: 10.3390/ijms23031023.
- [14] Y. Wen, J. Yuan, X. Ma, S. Wang and Y. Liu, "Polymeric nanocomposite membranes for water treatment: A review," *Environ. Chem. Lett.*, vol. 17, no. 4, pp. 1539–1551, May 2019, doi: 10.1007/s10311-019-00895-9.
- [15] B. Guo, Q. Yin, J. Zhou, W. Li, K. Zhang and Y. Li, "Semiconductive polymer-doped PEDOT with high work function, conductivity, reversible dispersion, and application in organic solar cells," *ACS Sustainable Chem. Eng.*, vol. 7, no. 9, pp. 8206–8214, April 2019, doi: 10.1021/acssuschemeng.8b06215.
- [16] J. Zhang *et al.*, "Reducing photovoltaic property loss of organic solar cells in blade-coating by optimizing micro-nanomorphology via nonhalogenated solvent," *Adv. Energy Mater.*, vol. 12, no. 14, p. 2200165, April 2022, doi: 10.1002/aenm.202200165.
- [17] J. Wan *et al.*, "Realizing high-performance organic solar cells through precise control of HOMO driving force based on ternary alloy strategy," *J. Energy Chem.*, vol. 65, pp. 133–140, February 2022, doi: 10.1016/j.jechem.2021.05.053.
- [18] Z. Su, L. Wang, Y. Li, H. Zhao, B. Chu and W. Li, "Ultraviolet-ozone-treated PEDOT:PSS as anode buffer layer for organic solar cells," *Nanoscale Res. Lett.*, vol. 7, no. 1, pp. 1–6, August 2012, doi: 10.1186/1556-276X-7-465.
- [19] M. Kaltenbrunner *et al.*, "Ultrathin and lightweight organic solar cells with high flexibility," *Nature Communications*, vol. 3, p. 770, April 2012, doi: 10.1038/ncomms1772.

- [20] S. Liu, Y. Sun, L. Chen, Q. Zhang, X. Li and J. Shuai, "A review on plasmonic nanostructures for efficiency enhancement of organic solar cells," *Mater. Today Phys.*, vol. 24, p. 100680, May 2022, doi: 10.1016/j.mtphys.2022.100680.
- [21] P. Shen, Y. Liu, Y. Long, L. Shen and B. Kang, "High-performance polymer solar cells enabled by copper nanoparticles-induced plasmon resonance enhancement," *J. Phys. Chem. C*, vol. 120, no. 16, pp. 8900–8906, April 2016, doi: 10.1021/acs.jpcc.6b02802.
- [22] Z. Liu, S. Y. Lee and E.-C. Lee, "Copper nanoparticle incorporated plasmonic organic bulk-heterojunction solar cells," *Appl. Phys. Lett.*, vol. 105, no. 22, December 2014, doi: 10.1063/1.4903749.
- [23] C.-L. Huang, G. Kumar, G. D. Sharma and F.-C. Chen, "Plasmonic effects of copper nanoparticles in polymer photovoltaic devices for outdoor and indoor applications," *Appl. Phys. Lett.*, vol. 116, no. 25, June 2020, doi: 10.1063/5.0010427.
- [24] A. Ng *et al.*, "Enhanced performance of PTB7:PC71BM solar cells via different morphologies of gold nanoparticles," *ACS Appl. Mater. Interfaces*, vol. 6, no. 23, pp. 20676–20684, November 2014, doi: 10.1021/am504250w.
- [25] Q. Li *et al.*, "Decahedral-shaped Au nanoparticles as plasmonic centers for high performance polymer solar cells," *Org. Electron.*, vol. 43, pp. 33–40, April 2017, doi: 10.1016/j.orgel.2017.01.010.
- [26] A. Iwan, B. Boharewicz, I. Tazbir, A. Sikora and B. Zboromirska-Wnukiewicz, "Silver nanoparticles in PEDOT:PSS layer for polymer solar cell application," *Int. J. Photoenergy*, vol. 2015, March 2015, doi: 10.1155/2015/764938.
- [27] J. Rivera-Taco *et al.*, "The role of silver nanoparticles in the hole transport layer in organic solar cells based on PBDB-T:ITIC," *J. Electron. Mater.*, vol. 50, no. 7, pp. 4118–4127, April 2021, doi: 10.1007/s11664-021-08919-3.
- [28] D. Duche *et al.*, "Improving light absorption in organic solar cells by plasmonic contribution," *Sol. Energy Mater. Sol. Cells*, vol. 93, no. 8, pp. 1377–1382, August 2009, doi: 10.1016/j.solmat.2009.02.028.
- [29] S. Vedraine et al., "Intrinsic absorption of plasmonic structures for organic solar cells," Sol. Energy Mater. Sol. Cells, vol. 95, pp. S57–S64, May 2011, doi: 10.1016/j.solmat.2010.12.045.
- [30] M. Dhonde, K. Sahu, V. V. S. Murty, S. S. Nemala and P. Bhargava, "Surface plasmon resonance effect of Cu nanoparticles in a dye sensitized solar cell," *Electrochim. Acta*, vol. 249, pp. 89–95, September 2017, doi: 10.1016/j.electacta.2017.07.187.
- [31] J. Chen *et al.*, "Solution-processed copper nanowire flexible transparent electrodes with PEDOT:PSS as binder, protector and oxide-layer scavenger for polymer solar cells," *Nano Res.*, vol. 8, no. 3, pp. 1017–1025, October 2015, doi: 10.1007/s12274-014-0583-z.

- [32] T. M. D. Dang, T. T. T. Le, E. Fribourg-Blanc and M. C. Dang, "The influence of solvents and surfactants on the preparation of copper nanoparticles by a chemical reduction method," *Adv. Nat. Sci.: Nanosci.*, vol. 2, no. 2, p. 025004, April 2011, doi: 10.1088/2043-6262/2/2/025004.
- [33] J. S. Nyarige, T. P. J. Krüger and M. Diale, "Structural and optical properties of hematite and L-arginine/hematite nanostructures prepared by thermal spray pyrolysis," *Surf. Interfaces*, vol. 18, p. 100394, March 2020, doi: 10.1016/j.surfin.2019.100394.
- [34] M. Samim, N. Kaushik and A. Maitra, "Effect of size of copper nanoparticles on its catalytic behaviour in Ullman reaction," *Bull. Mater. Sci.*, vol. 30, no. 5, pp. 535–540, November 2007, doi: 10.1007/s12034-007-0083-9.
- [35] J. Suárez-Cerda, H. Espinoza-Gómez, G. Alonso-Núñez, I. A. Rivero, Y. Gochi-Ponce and L. Z. Flores-López, "A green synthesis of copper nanoparticles using native cyclodextrins as stabilizing agents," *J. Saudi Chem. Soc.*, vol. 21, no. 3, pp. 341–348, March 2017, doi: 10.1016/j.jscs.2016.10.005.
- [36] T. Thirugnanasambandan and M. Alagar, "X-ray diffraction studies of copper nanopowder," *Arch. Phys. Res.*, vol. 1, March 2010.
- [37] A. J. Olivares *et al.*, "Nanostructural modification of PEDOT:PSS for high charge carrier collection in hybrid frontal interface of solar cells," *Polymers*, vol. 11, no. 6, doi: 10.3390/polym11061034.
- [38] P. V. Almeida, C. Izumi, H. F. D. Santos and A. C. Sant'Ana, "Spectroscopic characterization of PEDOT:PSS conducting polymer by resonance Raman and SERRS spectroscopies," *Quím. Nova*, vol. 42, no. 9, pp. 1073–1080, October 2019, doi: 10.21577/0100-4042.20170417.
- [39] Y. Su, S. Qiu, Y. Liu, D. Yang, H. Zhao and L. Wang, "PEDOT: PSS-exfoliated graphene to improve the corrosion resistance of waterborne epoxy coating," *Int. J. Electrochem. Sci*, vol. 14, no. 5, pp. 4595–4610, May 2019, doi: 10.20964/2019.05.37.
- [40] S. Xiong, L. Zhang and X. Lu, "Conductivities enhancement of poly(3,4-ethylenedioxythiophene)/poly(styrene sulfonate) transparent electrodes with diol additives," *Polym. Bull.*, vol. 70, pp. 237–247, August 2012, doi: 10.1007/s00289-012-0833-8.
- [41] P. Veerender *et al.*, "Probing the annealing induced molecular ordering in bulk heterojunction polymer solar cells using in-situ Raman spectroscopy," *Sol. Energy Mater. Sol. Cells*, vol. 120, part B, pp. 526–535, January 2014, doi: 10.1016/j.solmat.2013.09.034.
- [42] F. Otieno et al., "Enhancement of organic photovoltaic device performance via P3HT:PCBM solution heat treatment," *Thin Solid Films*, vol. 625, pp. 62–69, March 2017, doi: 10.1016/j.tsf.2017.01.047.

- [43] A. Yadav, A. Upadhyaya, S. Gupta, A. Verma and C. Mohan, "Solution processed graphene as electron transport layer for bulk heterojunction based devices," *Superlattices Microstruct.*, vol. 120, August 2018, doi: 10.1016/j.spmi.2018.06.037.
- [44] P. Khanna, P. More, J. Jawalkar, Y. Patil and N. K. Rao, "Synthesis of hydrophilic copper nanoparticles: Effect of reaction temperature," *J. Nanoparticle Res.*, vol. 11, no. 4, pp. 793–799, June 2009, doi: 10.1007/s11051-008-9441-9.
- [45] L. Q. Pham *et al.*, "Copper nanoparticles incorporated with conducting polymer: Effects of copper concentration and surfactants on the stability and conductivity," *J. Colloid Interface Sc.*, vol. 365, no. 1, pp. 103–109, January 2012, doi: 10.1016/j.jcis.2011.09.041.
- [46] M. Muniz-Miranda, C. Gellini and E. Giorgetti, "Surface-enhanced Raman scattering from copper nanoparticles obtained by laser ablation," *J. Phys. Chem. C*, vol. 115, no. 12, pp. 5021–5027, January 2011, doi: 10.1021/jp1086027.
- [47] M. Ismail, "Green synthesis and characterizations of copper nanoparticles," *Mater. Chem. Phys.*, vol. 240, p. 122283, January 2020, doi: 10.1016/j.matchemphys.2019.122283.
- [48] F. Otieno *et al.*, "Improved efficiency of organic solar cells using Au NPs incorporated into PEDOT:PSS buffer layer," *AIP Adv.*, vol. 7, no. 8, p. 085302, August 2017, doi: 10.1063/1.4995803.
- [49] M. Shaban, M. Benghanem, A. Almohammedi and M. Rabia, "Optimization of the active layer P3HT:PCBM for organic solar cell," *Coatings*, vol. 11, no. 7, p. 863, July 2021, doi: 10.3390/coatings11070863.
- [50] G. Hassan, M. Sajid and C. Choi, "Highly sensitive and full range detectable humidity sensor using PEDOT:PSS, methyl red and graphene oxide materials," *Sci. Rep.*, vol. 9, no. 1, p. 15227, October 2019, doi: 10.1038/s41598-019-51712-w.